

# Protein Corona and Immune Responses of Borophene: A Comparison of Nanosheet–Plasma Interface with Graphene and Phosphorene

Miaomiao Han, Longqian Zhu, Jianbin Mo, Wei Wei, Biao Yuan, Jing Zhao,\* and Chongqiang Cao\*

Cite This: *ACS Appl. Bio Mater.* 2020, 3, 4220–4229

Read Online

ACCESS |

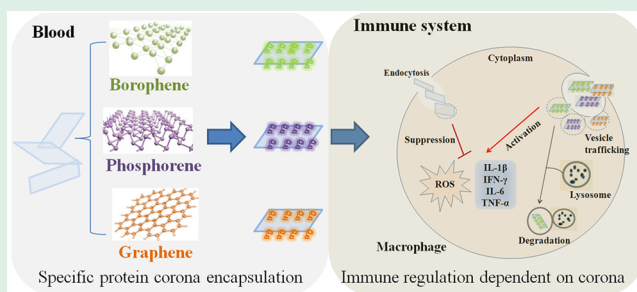
Metrics & More

Article Recommendations

Supporting Information

**ABSTRACT:** Borophene has emerged as a type of two-dimensional monoelemental nanomaterials with excellent drug loading capacity and photothermal properties. Here, we demonstrated the adsorption of plasma proteins onto borophene nanosheets (B NSs) and the promoted immune responses of macrophage by the B NS–corona complex. We discovered that plasma proteins changed the surface identities of B NSs. Using proteomics analysis, 46.5% of the proteins bound to B NSs (94 plasma proteins) were immune-relevant proteins. Uptake of B NSs by phagolysosomes was observed, and the plasma corona promoted the uptake. In comparison with graphene and phosphorene, we found that 32 plasma proteins appeared on all of the three nanosheets. The proportion of immune-relevant proteins in graphene–corona and phosphorene–corona was 41.3% and 75.6%, respectively. The components of the adsorbed immune-relevant proteins show diversity, which influence the immune responses of these nanosheets. Phosphorene–corona showed the most remarkable immunoregulatory behavior in these nanosheets. For the first time, we compared the highly complex protein corona at the nanosheet–plasma interface of three key 2D monoelemental nanosheets. Our study helps to understand the interaction between borophene and biological systems and provides a theoretical basis for the development and application of borophene in the biomedical field.

**KEYWORDS:** borophene, phosphorene, protein corona, plasma proteins, immune response



## INTRODUCTION

Borophene, as a type of two-dimensional (2D) monoelemental nanomaterials (Xenes), has recently attracted wide attention in the fields of energy, environment, chemistry, and biomedicine due to its excellent morphological structure and physicochemical property.<sup>1–8</sup> Xenes (especially graphene and phosphorene) with excellent photothermal conversion and drug loading capability have been widely reported for photothermal therapy and drug delivery research.<sup>9–14</sup> Compared with graphene and phosphorene, borophene has shown more considerable potential for the biomedical field, owing to its particular tractability and good biocompatibility.<sup>11</sup> Pioneering studies by Zhang, Mei, and Shi et al. showed that ultrathin borophene nanosheets exhibited multiple promising features for imaging-guided cancer therapy.<sup>15</sup> Many studies have focused on the applications of borophenes in biomedicine. However, molecular understanding on the biological consequences of this nanomaterial in physiological environments is limited.

Only nanomaterials enter organisms, and they inevitably come into contact with biological tissue and absorb large amounts of biomolecules.<sup>16</sup> It has been proven that nanomaterials are coated by plasma protein (termed the “protein corona”) when nanomaterials are surrounded by blood.<sup>17</sup> Chen

et al. reported that “protein corona” changes the identity of nanomaterials in the organism, which determines the cellular uptake, toxicity, and immune response of nanomaterials.<sup>18–21</sup> Therefore, the biological effects of nanomaterials are not just influenced by the properties of the nanomaterials themselves.<sup>22–24</sup> Considering the great potential of borophene nanomaterials in biomedical applications, it is critically important to systematically evaluate the interactions between borophenes and blood system and the influence of plasma protein on the immune regulation behaviors of borophene nanomaterials.

In this work, we have synthesized borophene nanosheets (B NSs) by a top-down liquid-phase exfoliation method and have chosen two representative Xenes, graphene nanosheets (GR NSs) and phosphorene nanosheets (BP NSs), as typical

Received: March 18, 2020

Accepted: May 28, 2020

Published: May 28, 2020



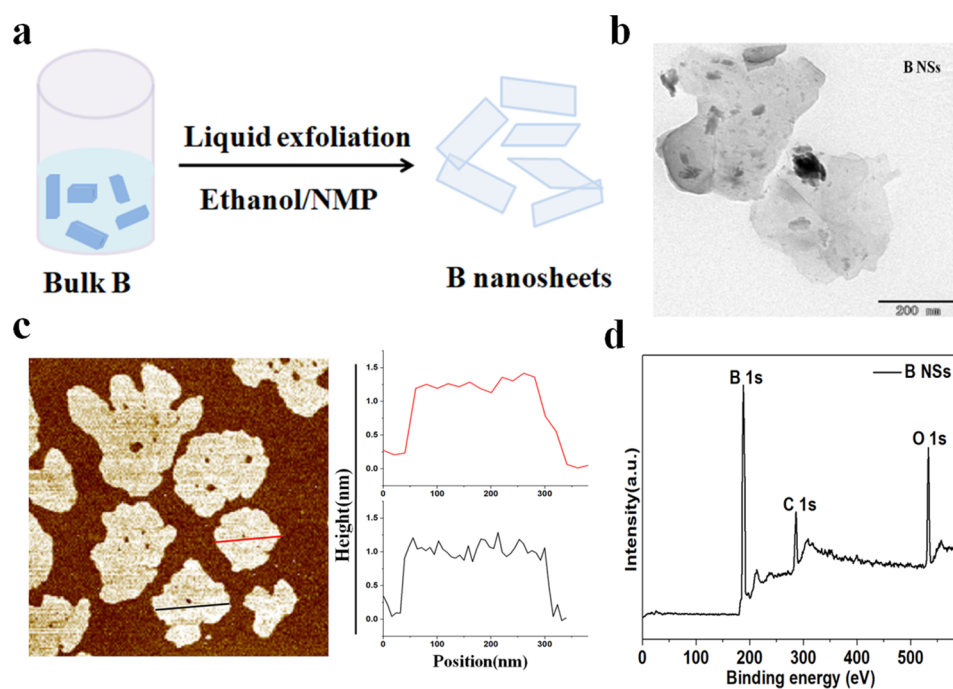


**Figure 1.** Preparation and characterization of B NSs. (a) Schematic diagram of B NSs were prepared by sonochemical exfoliation, not drawn to scale. (b) TEM images of B NSs. (c) AFM images of B NSs, the colored lines represent the height. (d) XPS spectra of B NSs.

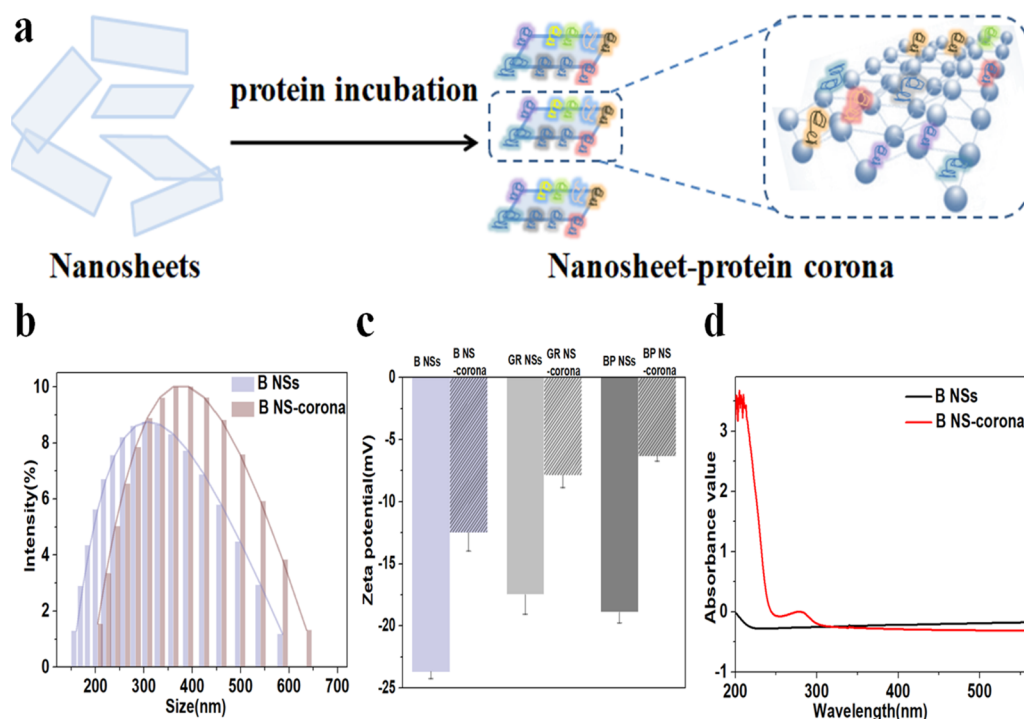


**Figure 2.** (a) Schematic representation of corona formation around B NSs, not drawn to scale. (b) Hydrodynamic size analysis of B NSs and B NS–corona complexes. (c)  $\zeta$  potentials of B NSs/GR NSs/BP NSs and the nanosheet–corona complexes. The data were calculated as mean  $\pm$  standard deviation. (d) UV–vis spectra of B NSs and B NS–corona complexes.

comparisons. We studied the protein corona by exposing B NSs to plasma proteins and demonstrated the immunoregulation of B NSs mediated by the blood-protein corona on macrophages. Our results highlighted that the protein corona could redefine the surface properties of B NSs and, subsequently, the biological responses.

## RESULTS AND DISCUSSION

**Characterization of Nanosheets and Corona Complexes.** B NSs were synthesized by an ultrasonication method (Figure 1a). The synthesized B NSs exhibited small nanosheet structures, which became dispersed in water by transmission electron microscopy (TEM) (Figure 1b). The thickness of B NSs was approximately 1.25 nm by AFM topographic (Figure

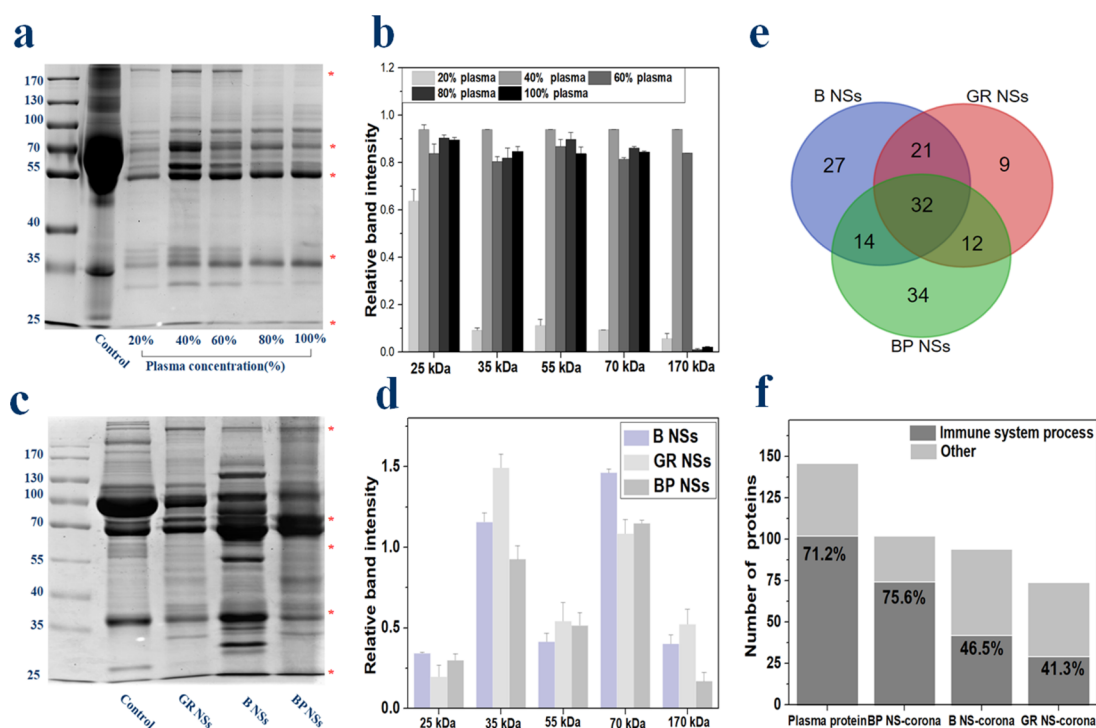


**Figure 3.** Protein corona composition and identification. (a) SDS-PAGE analysis of plasma protein and B NS–corona complexes in the different concentrations of plasma proteins. (b) Relative amounts of the most abundant proteins the surface of B NS–corona in the different concentrations of plasma proteins. (c) SDS-PAGE picture of protein corona from GR NSs/B NSs/BP NSs. (d) Relative amounts of plasma proteins adsorbed by GR NSs/B NSs/BP NSs. The data were calculated as mean  $\pm$  standard deviation. (e) Number of proteins on nanosheet–corona complexes identified by LC–MS/MS. (f) Number of proteins on nanosheet–corona complexes involved in immune process according to GO analysis.

1c). X-ray photoelectron spectroscopy (XPS) indicated that all peaks of B NSs in these spectra matched well with the reported results.<sup>2</sup> Elemental analysis showed that B NSs contain 70.64% boron, 11.03% carbon, and 18.34% oxygen, indicating high purity of B NSs synthesized (Figure 1d). Small amounts of carbon and oxygen come from solvents and air impurities. Scanning electron microscopy (SEM) was used to evaluate the size distribution of B NSs. The result suggested that B NSs were free-standing with a size of around  $319 \times 290 \text{ nm}^2$  (Figure S2). Dynamic light scattering (DLS) results indicated that the hydrodynamic sizes of B NSs, GR NSs, and BP NSs are similar, approximately 320 nm (Figure S3). The  $\zeta$  potential tests show that three nanosheets have negative charges (Figure 2c). It has been reported that the carbon–carbon bond between the carbon atoms of graphene is hybridized with a  $sp^2$  orbital, so its mechanical strength and chemical stability are very high, and it can exist stably in the atmosphere without being easily oxidized.<sup>25,26</sup> Boron, as the fifth element, has a carbon-like  $sp^2$  hybrid orbital, a short covalent bond radius, and a variety of valence states, which are conducive to the formation of stable low-dimensional borophene.<sup>6,8</sup> Previous studies have shown that B NSs have high stability at room temperature and are oxidized only at high temperature (more than  $600^\circ\text{C}$ ), and the oxidation of B NSs was found to occur at the edges of the nanosheets, and the terrace of B NSs remains almost intact.<sup>15</sup> However, phosphorenes are not as stable as graphene and borophene. It has been shown that phosphorene nanomaterials are prone to reactions between water and oxygen in the environment, leading to nanomaterials degradation.<sup>27–29</sup> Phosphorene's unique honeycombed fold structure allows for one phosphorus atom to covalently bond with three other monolayer phosphorus atoms, thereby exposing a lone pair of

electrons. The lone pair electrons are easy to react with oxygen to form  $PxOy$ , which is soluble in water.  $P^0$  on the exposed surface is further oxidized, resulting in phosphorene degradation.<sup>29,30</sup>

Some studies have reported the characterization of the corona on GR NSs or BP NSs,<sup>31,32</sup> but B NS–corona have rarely been studied. Therefore, to study the effect of protein corona on the biological identity of B NSs, we compared the characterization of B NSs and B NS–corona complexes, including the morphology features, UV–vis spectral characteristics, size distribution, and  $\zeta$  potential (Figure 2a). TEM images of B NS–corona complexes showed that B NSs are coated with a transparent protein corona film (Figure S1). The UV–vis spectra indicated that protein absorption peaks were present in the B NS–corona complexes (Figure 2d). B NS–corona complexes were strikingly different from bare B NSs forms; the  $\zeta$  potential value decreased from  $-23.7$  to  $-12.5 \text{ mV}$  (Figure 2c), suggesting encapsulation of plasma proteins onto the surface of B NSs and the improved stability of B NSs in suspension. The hydrodynamic size of B NSs increased from  $318.6 \pm 2.3$  to  $393.5 \pm 5.9 \text{ nm}$  by DLS (Figure 2b). To evaluate the influence of corona adsorption on nanosheets stability, bare nanosheets and the nanosheet–corona complexes with the same amount of concentration were dispersed in water and exposed to air for 7 days and then their hydrodynamic size were tested within a predetermined time. The hydrodynamic size of these nanosheet–corona complexes in air and water was further monitored (Figure S4). It can be observed that the size of these nanosheets had no significant change. These results demonstrated that protein corona adsorption could effectively prevent the degradation of these nanosheets and maintain good stability in water and air.

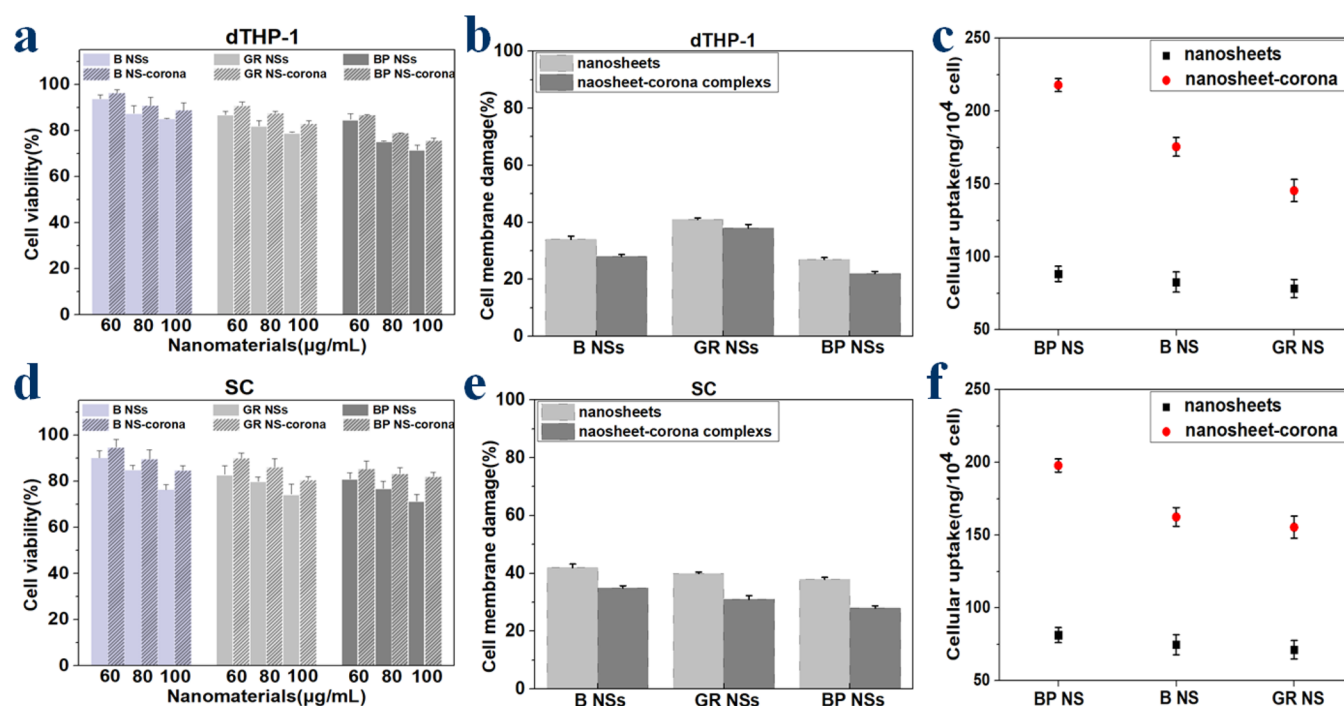


**Figure 4.** In vitro cytotoxicity and uptake of nanosheets and corona complexes. (a and d) Cell viability: Cells were treated with B NSs/GR NSs/BP NSs and the nanosheet–corona complexes (60, 80, and 100  $\mu\text{g/mL}$ ) for 24 h. The data were calculated as mean  $\pm$  standard deviation. (b and e) Cell membrane damage: Cells were treated with B NSs/GR NSs/BP NSs and the nanosheet–corona complexes at 100  $\mu\text{g/mL}$  for 24 h. The data were calculated as mean  $\pm$  standard deviation. (c and f) Cellular uptake: Cells were treated with B NSs/GR NSs/BP NSs and the nanosheet–corona complexes at 200  $\mu\text{g/mL}$  for 6 h. The data were calculated as mean  $\pm$  standard deviation.

**Composition and Identification of Plasma Protein Corona.** To further analyze the composition of plasma proteins encapsulated on B NSs and understand the difference in plasma proteins adsorbed by different 2D mono-elemental nanosheets, B NSs were placed in different concentrations of blood plasma. Sodium dodecyl sulfate–polyacrylamide gel electrophoresis (SDS–PAGE) was used to characterize plasma protein corona. The relative strength of the bands in the electrophoresis results was analyzed by the relative densitometry. As blood plasma concentration increases, typical bands from the B NS–corona become gradually more visible; after the plasma concentration increased to 40%, the proteins bands strength did not increase (Figure 3a,b). Then, these nanosheets were exposed to 40% blood plasma. Typical bands (25, 35, 55, 70, and 170 kDa proteins) dominate the protein corona composition in three nanosheet–corona complexes (Figure 3c,d). Furthermore, the adsorption capacities of these NSs were measured by BCA assay (Figure S5). It was found that these nanosheets can adsorb an amount of plasma proteins:  $\sim 0.349 \mu\text{g}$  of plasma proteins per  $\mu\text{g}$  of BP NSs,  $\sim 0.246 \mu\text{g}$  of plasma proteins per  $\mu\text{g}$  of B NSs, and  $\sim 0.179 \mu\text{g}$  of plasma proteins per  $\mu\text{g}$  of GR NSs. These results suggested BP NSs have stronger plasma protein adsorption capacity than do GR NSs and B NSs.

Further, liquid chromatography tandem mass spectrometry (LC–MS/MS) was employed to qualitatively analyze the composition of these nanosheet–corona complexes.<sup>33</sup> We observed that proteins  $<70$  kDa accounted for the majority of the protein corona components of three nanosheets (Figure S6). In addition, of the plasma proteins bound to B NSs, more than half of the plasma proteins (63.71%) had negative charge (isoelectric point (pI)  $<7.0$ ) (Figure S7). The charge distribution of proteins bound to GR NSs and BP NSs shows a similar pattern. This result is also reflected by  $\zeta$  potential of

these nanosheet–corona complexes, which display negative charge.

Previous studies suggested that the protein corona consists of a few tens of proteins in human blood plasma.<sup>33–35</sup> Further MS analysis revealed that B NSs were able to adsorb 94 plasma proteins, accounting for 63.38% of the total plasma proteins (Figure 3e). Of these proteins, 32 proteins appeared on the three nanosheets, indicated by presumably leading to similarity in their biological response to the physiological environment. Table S1 further lists the 20 abundant plasma proteins for three nanosheets at the same time point; serum albumin and fibrinogen were found to be the main components of protein corona for the three nanosheet–corona complexes. This result could be attributed to serum albumin and fibrinogen, which are both relatively abundant in plasma.<sup>36</sup> In addition, immunoglobulin, apolipoproteins, and complement C3 are also enriched in the three nanosheet–corona complexes. These results indicated that the protein components adsorbed by these nanosheets were related to the protein abundance in plasma. The protein corona was further classified by gene ontology (GO) analysis according to their biological process. Protein corona (46.5%) adsorbed by B NSs (94 plasma proteins) were immune-related proteins; the percentage for GR NS/BP NS–corona complexes (74 and 102 plasma proteins, respectively) was 41.3% and 75.6% (Figure 3f). The complete data sets are provided in Tables S2, S3, and S4. Immune proteins are the main factors of innate immunity in vivo and have positive and negative effects on the immune response.<sup>37</sup> Compared with B NSs and GR NSs, BP NSs adsorb more immune proteins. This effect may cause differences in the immune response of immune cells to these nanosheets.

**In Vitro Cytotoxicity and Uptake Study for Nanosheets and Corona Complexes.** The toxicological profile of nanomaterials is an important obstacle for biomedical

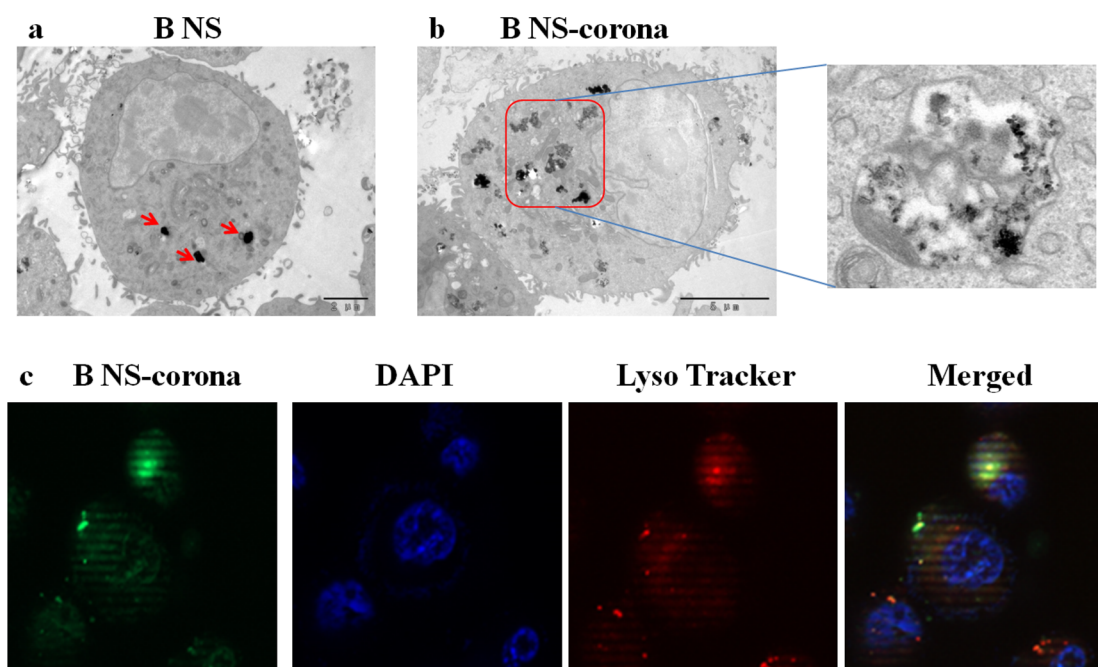


**Figure 5.** Cellular internalization of B NSs and B NS–corona complexes. (a and b) TEM images of dTHP-1 after exposure to B NSs and B NS–corona complexes for 6 h, washed with PBS three times. (c) Inverted fluorescence microscope images of dTHP-1 after exposure to B NS–corona complexes for 6 h, washed with PBS three times and stained.

trials.<sup>38–40</sup> It is critical to understand how the biomolecules in different biological milieu impact the toxicity of nanomaterials. Nanomaterials exposed to biological system are first recognized by monocytes and macrophages.<sup>41</sup> Therefore, the toxicity of these NSs and NS–corona complexes to human macrophage-like cells (dTHP-1 cells) and macrophages from peripheral blood (SC cells) was first investigated in the following experiment. Cytotoxicity was assessed by the MTT assay, and membrane damage was assessed by the lactate dehydrogenase (LDH) activity assay (Figure 4). After treatment with 100  $\mu\text{g}/\text{mL}$  B NSs and B NSs–corona complexes, the viability of dTHP-1 cells was 84.2% and 88.5%, respectively, and the viability of SC cells was 76.3% and 84.7%, respectively. The dTHP-1 cells membranes damaged upon treatment at a high concentration of B NSs and B NSs–corona complexes (100  $\mu\text{g}/\text{mL}$ ) were 34% and 28%, respectively, and the SC cells membranes damaged were 42% and 35%, respectively. These results suggested that these NSs can damage the cell membrane due to the hydrophobic forces between these NSs and the phospholipids.<sup>42–44</sup> Macrophages cell membrane damage and cytotoxicity decreased when cells were exposed to these NSs–corona complexes, suggesting that protein corona play an important role in reducing cytotoxicity and membrane damage for macrophages.

To further analyze the effect of protein corona on cellular uptake, the uptake efficiency of B NSs, GR NSs, BP NSs, and these corona complexes in dTHP-1 cells and SC cells was investigated by inductively coupled plasma mass spectrometry (ICP-MS). Our results showed that protein corona promotes the phagocytosis of these NSs by macrophages. The adsorption of immune-related proteins onto the surface of these NSs might be recognized by receptors on the macrophages, promoted by the internalization of these NS–corona complexes. Additionally, cellular uptake of BP NS–corona complexes (217.5 ng per  $10^4$  dTHP-1 cells) was higher than that of B NS–corona complexes (174.9 ng per  $10^4$  dTHP-1 cells) and GR NS–corona complexes

(135.2 ng per  $10^4$  dTHP-1 cells). The more immune-related proteins in BP NS–corona complexes and the high expression of receptors in macrophages<sup>44</sup> could contribute to the high internalization of BP NS–corona complexes.

**Intracellular Location of Nanosheets and Corona Complexes.** To further investigate the intracellular location of B NSs and the corona complexes, the cellular track of B NSs and the corona complexes were performed using TEM. The cellular internalization of GR NSs and BP NSs has been confirmed to be an endocytic pathway and thus to be located in the cytoplasm.<sup>32,45</sup> Representative TEM micrographs are shown in Figure 5a. This result is consistent with the cellular internalization of GR NSs and BP NSs. After 6 h of exposure, the cells contained intracellular B NSs, which were observed within membrane-bound organelles, suggesting that B NSs were identified as having been effectively endocytosed. The corona complexes exhibit the same endocytic pathway (Figure 5b). In previous studies, we constructed stable fluorescent plasma complexes by using human serum albumin conjugated to fluorescein isothiocyanate (HSA-FITC) to plasma.<sup>32</sup> This method facilitates the monitoring of the position of the fluorescently labeled B NS–corona complexes within dTHP-1 cells. Inverted fluorescence microscope was used to study the intracellular location of B NS–corona complexes (Figure 5c). The final location of B NS–corona complexes was the cell cytoplasm. Both bare B NSs and the corona complexes were phagocytic through endocytosis into macrophages and aggregates into irregular clusters in lysosomes spread throughout the cell cytoplasm. This result indicates that the mono-elemental nanosheets with similar characteristics may have the same cellular internalization pattern.

**Proinflammatory Effects of NSs–Corona Complexes.** Various nanomaterials have been reported to stimulate macrophages to produce inflammatory cytokines.<sup>46</sup> Studies have shown that the formation of protein corona on the surface of nanomaterials is the main trigger for the inflammatory response

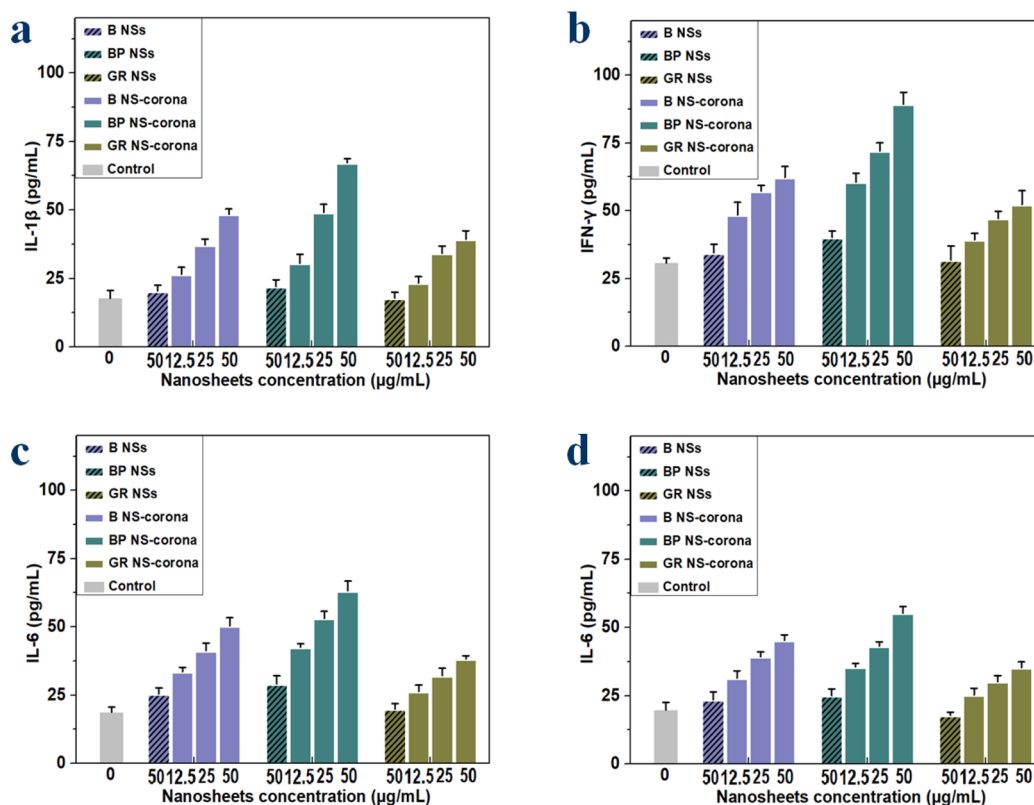


**Figure 6.** Cytokine secretion of dTHP-1 cells. (a–d) Macrophage-like dTHP-1 cells were incubated with these NSs (50  $\mu\text{g/mL}$ ) and the different concentrations of NS–corona complexes (12.5, 25, and 50  $\mu\text{g/mL}$ ) for 12 h. The data were calculated as mean  $\pm$  standard deviation.

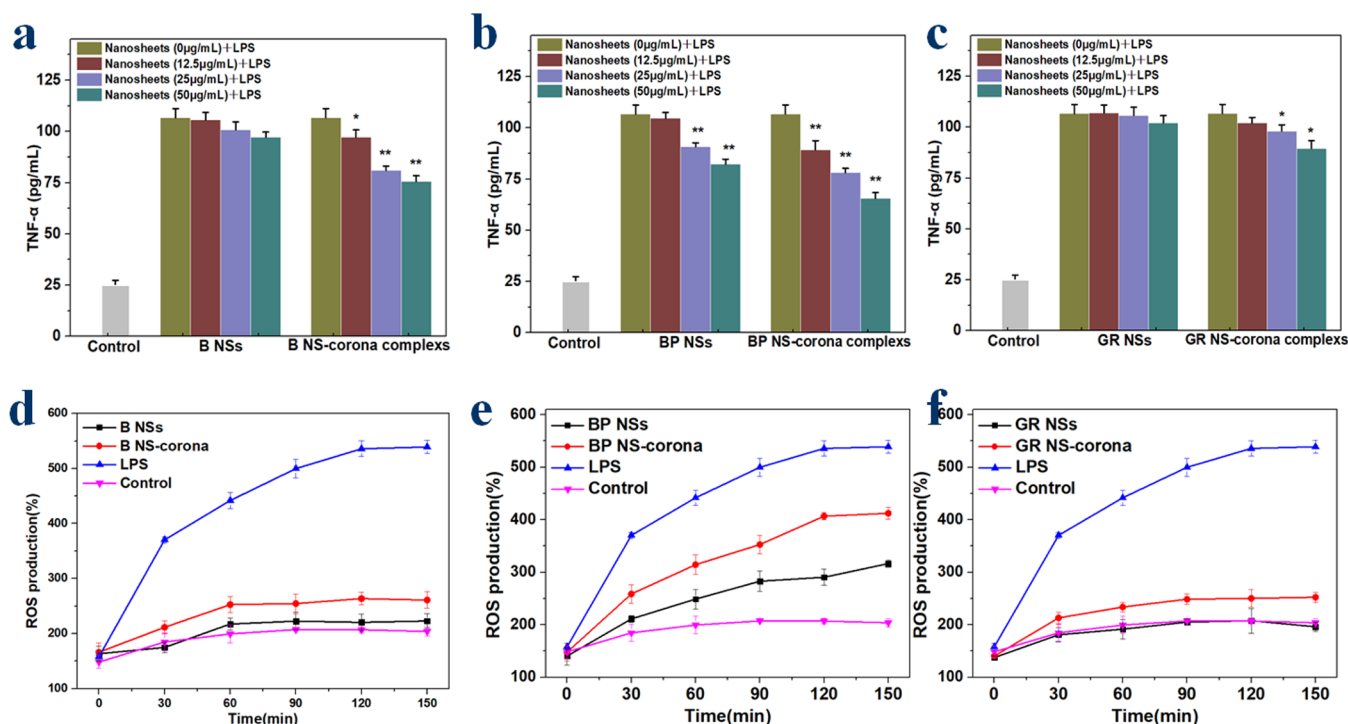


**Figure 7.** Immune regulation of NS–corona complexes in macrophages. (a–c) TNF- $\alpha$  secretion in dTHP-1 cells. LPS (20 ng/mL) was added to dTHP-1 cells, which had been pretreated with B NSs/BP NSs/GR NSs or the NS–corona complexes for 12 h. The data were calculated as mean  $\pm$  standard deviation. \* $p$  < 0.05, \*\* $p$  < 0.01. (d–f) ROS production in dTHP-1 cells. dTHP-1 cells were treated with 50  $\mu\text{g/mL}$  NSs or the NS–corona complexes for 12 h. LPS was set as the control. The data were calculated as mean  $\pm$  standard deviation.

of nanomaterials.<sup>47–49</sup> To investigate the inflammatory response of these NS–corona complexes, macrophage-like cells were

incubated with either NSs or NS–corona complexes (Figure 6, Figure S8). Then, inflammatory cytokines in the cells culture

supernatants, including interleukin (IL)-1 $\beta$ , IL-6, IL-8, and interferon (IFN)- $\gamma$  were measured by enzyme-linked immunosorbent assay (ELISA). When treated with B NS–corona complexes, the cytokine secretion changed significantly in dTHP-1 cells. Protein corona stimulates the secretion of inflammatory cytokines to increase significantly, 1–2 folds above the untreated group. B NSs did not stimulate significant changes in cytokines. Moreover, the expression of inflammatory cytokines in SC cells has a similar phenomenon. By comparing with GR NS/BP NS–corona complex, we found that BP NS–corona complexes promoted a greater release of cytokines than B NS/GR NS–corona complexes. After 12 h of treatment with BP NS–corona complexes (50  $\mu$ g/mL), the level of IFN- $\gamma$  (87.5 pg/mL) in macrophage-like dTHP-1 cells was the highest among these NS–corona complexes. These results suggest that the protein corona plays an important role in promoting the inflammatory response of these nanosheets. Of the three nanosheets–corona complexes, BP NS–corona complexes have the strongest proinflammatory effect on macrophages.

**Immune Regulation of NSs–Corona Complexes in Macrophages.** Toxic or subtoxic nanomaterials can disrupt the immune response of macrophages by regulating cytokine levels.<sup>50</sup> The tumor necrosis factor (TNF- $\alpha$ ) produced by macrophages is an important cytokine marker for the immune response.<sup>51,52</sup> In order to study the immune regulation behavior of these NS–corona complexes on macrophages, lipopolysaccharide (LPS) was used to induce macrophages to produce cytokines to model inflammation. We studied the immune response in dTHP-1 cells caused by these NSs and the NS–corona complexes (Figure 7a–c). The protein corona significantly inhibited TNF- $\alpha$  secretion in LPS-treated dTHP-1 cells. dTHP-1 cells were pretreated with the different concentrations of B NS–corona complexes and then incubated with LPS; the secretion of TNF- $\alpha$  was significantly decreased to 74.33 from 106.19 pg/mL (without pretreatment with B NS–corona complexes). But, B NSs did not cause significant changes in TNF- $\alpha$ . It followed that B NS–corona complexes could affect the response of macrophages to foreign materials. Similarly, GR NSs elicit the immune response from macrophages only in the presence of the protein corona. These results supported that protein corona perturb the immune response of macrophages.

Reactive oxygen species (ROS) is an important part of the original immune response of macrophages to foreign substances, and the expression of ROS has also been recognized as a major immunotoxicity indicator of nanomaterials,<sup>53</sup> ROS overexpression implies enhanced immunotoxicity. The ROS level induced by these NSs and the NS–corona complexes was measured with the fluorescent probe DCFH-DA (Figure 7d–f). Compared with B NSs, B NS–corona complexes induced a much higher ROS production. After 120 min of exposure, increases of 48% in ROS levels were observed in B NS–corona complexes treatment groups, compared with B NSs treatment groups. ROS production was significantly increased in dTHP-1 cells treated with BP NSs or BP NS–corona complexes. BP NSs and BP NS–corona complexes induced ROS overproduction in dTHP-1 cells at approximately 335.1% and 421.2% at 150 min, which were higher than the control group (215.7%). These results suggested that these NSs exhibited catalytic immunotoxicity and immune regulation in macrophages due of the formation of plasma corona.

## CONCLUSION

The present study provides the first comprehensive investigations on the protein corona of borophenes formed in plasma and its influence on the cellular internalization and immune response in macrophages. Our results suggest that the participation of plasma proteins changes the surface characterizations of B NSs, mainly the sizes and  $\zeta$  potentials. Serum albumin and fibrinogen are the main components of the protein corona for B NS–corona complexes. Immunoglobulin and apolipoproteins are also enriched in B NS–corona complexes. A total of 46.5% of the proteins bound to B NSs (94 plasma proteins) were immune-related proteins. Bare B NSs and the corona complexes were phagocytic through endocytosis into macrophages and aggregate into irregular clusters in lysosomes. Bare B NSs do not provoke the immune response from macrophages, and the protein corona endows B NSs with proinflammatory and immunoregulatory activity. Our study provides a reliable reference for the research and development of borophene in nanomedicine.

Our comparison studies on borophenes, graphenes, and phosphorenes indicate that the 2D monoelemental nanosheets share common characteristics by showing similar surface changes in the blood system. The protein components adsorbed by these nanosheets were related to the protein abundance in plasma. Of the three nanosheets, phosphorenes adsorbed the most kinds of plasma proteins (involving immune proteins). In addition, these 2D monoelemental nanosheets with similar characteristics may have the same cellular internalization pattern. GR NSs and B NSs had immunoregulation behaviors only in the presence of plasma corona, while BP NSs had stronger immunoregulation behavior regardless of the absence and presence of corona. Our discovery suggests that highly complex protein corona formed rapidly at the nanosheet–plasma interface, which might be important to understand the toxicology of 2D monoelemental nanosheets.

## EXPERIMENTAL SECTION

**Material and Cell Lines.** Boron (B) powder was purchased from MACKLIN Chemical Co. Ltd. Suzhou, China. Black phosphorus powder were purchased from HWRK Chemical Co. Ltd. Beijing, China. Graphene nanosheets were purchased from Xian Feng Nano Technology Co. Ltd. Nanjing, China. *N*-Methyl pyrrolidone (NMP) was purchased from Aladdin Chemistry Co., Ltd. Shanghai, China. HSA-FITC was purchased from Biosynthesis Biotechnology Co., Ltd. Beijing, China. Human monocytic leukemia cells (THP-1 cells) and human macrophages from peripheral blood (SC cells) were purchased from the American Type Culture Collection, American. All of the cell lines were authenticated by STR typing and confirmed to be mycoplasma-free by Key GENBio TECH Co., Ltd. Nanjing, China.

**Preparation of B NSs and BP NSs.** B NSs were synthesized according to previous reports with slight changes.<sup>15</sup> Briefly, the boron powder with a concentration of 5 mg/mL was dispersed in a mixture of ethanol and NMP (1:1 v/v). The suspension was stripped by ultrasound through the probe for 48 h at 600 W and centrifuged at 6000 rpm for 20 min to remove the unstripped boron powder. Next, the retained supernatant was centrifuged at 12 000 rpm for 30 min and cleaned three times with ethanol. The precipitate is suspended in an aqueous solution at a fixed concentration. BP NSs were prepared according to previous reports.<sup>32</sup>

**Nanosheets and Plasma Proteins Interaction.** Plasma protein solution was derived from previous reports.<sup>32</sup> GR NSs/B NSs/BP NSs were incubated with a fixed concentration of plasma protein solution at 4  $^{\circ}$ C for 4 h. The solution was then centrifuged at 8000 rpm for 30 min at 4  $^{\circ}$ C so that the nanosheet–corona complexes could be obtained. The obtained complexes were washed three times with PBS to remove

the soft protein corona from the surface and were eventually suspended in PBS.

**Characterization of Nanosheets.** B NSs/GR NSs/BP NSs and the nanosheet–corona complexes solutions were separately dispersed on the carbon films attached with copper meshes, and then the surface morphologies were observed by JEOL JEM-1200EX TEM after air drying. B NSs were placed on the newly stripped mica sheet and dried with nitrogen, and the dried mica sheet was then imaged through Multimode M-Pico AFM. B NSs were placed on silicon substrates coated with Au and imaged through Hitachi SU-8220 high-resolution SEM. The average size of B NSs was measured using ImageJ software.

**ζ Potential and DLS Measurement.** These nanosheets and the corona complexes were suspended in PBS. The ζ potential was measured by a Nano-ZS instrument. The hydrodynamic diameter was measured through DLS. All experiments were performed three times to ensure repeatability of the results.

**Protein Corona Identification and Analysis.** Protein corona was separated by 12% SDS-PAGE. Then, the proteins strips were visualized by staining with Coomassie brilliant blue R-250. All experiments were performed three times to ensure repeatability of the results. Protein corona identification was performed by reference to previous experiments.<sup>32</sup> Briefly, after the separation of protein corona by SDS-PAGE. The proteins strips were extracted from the gel and then reduced, alkylated, and digested with trypsin. The obtained peptides were analyzed through nano-LC–MS/MS. The MS/MS spectra were searched using the MASCOT engine. The identified proteins were retrieved from the UniProtKB human database in FASTA format. Target proteins were performed by the GO analysis. All experiments were performed three times to ensure repeatability of the results.

**Cytotoxicity and Membrane Damage in Vitro.** Macrophages were seeded at a density of  $2 \times 10^4$  cells per well in a 96-well culture plate for 24 h, and then, the medium was replaced with 100 μL of serum-free medium containing different concentrations of nanosheets or the corona complexes (60, 80, and 100 μg/mL) for 24 h. Cytotoxicity was determined by MTT assay. Briefly, the treated cells were washed with PBS three times and then incubated with 100 μL of PBS (including 10% MTT) for 3 h. The resulting formazan crystals were dissolved in 110 μL of DMSO. Finally, PBS was removed and 100 μL of DMSO was added to dissolve the MTT crystals. The absorbance of DMSO solution was measured at 490 nm by an enzyme marker. Cell membrane damage was measured by LDH activity assay. Briefly, after the cells were exposed to these nanosheets or the corona complexes at 100 μg/mL for 24 h, the absorbance of the medium supernatant was determined at 490 nm. All experiments were performed three times to ensure repeatability of the results.

**In Vitro Cell Uptake Study.** Macrophages were seeded at a density of  $1.2 \times 10^6$  cells per well in a 6-well culture plate for 24 h. Cells were incubated with these nanosheets or the corona complexes at 200 μg/mL for 6 h. The medium was then removed, and the cells were washed multiple times with PBS in order to remove the remaining nanosheets or the corona complexes. One milliliter of 0.1 M NaOH solution (contained 1% Triton X-100) was added to lyse the cells. Next, the B, P, and C content in the lysates was determined by ICP-MS. All experiments were performed three times to ensure repeatability of the results.

**Intracellular Location of Nanosheets and Corona Complexes.** For TEM, macrophages were seeded at a density of  $1.2 \times 10^6$  cells per well in a 6-well culture plate for 24 h. Cells were incubated with these nanosheets or the corona complexes at 200 μg/mL for 6 h. The medium was then removed, and the cells were washed multiple times with PBS in order to remove the remaining nanosheets or the corona complexes. The cells were then immersed in the fixative and stained, sectioned, and imaged by TEM. All experiments were performed three times to ensure repeatability of the results.

For fluorescent imaging, macrophages were seeded at a density of  $6 \times 10^4$  cells per well in a 2 cm culture dish for 24 h. Cells were incubated with fluorescent labeled corona complexes for 6 h at 37 °C. The medium was then removed, and the cells were washed multiple times with PBS in order to remove the remaining fluorescent labeled corona complexes. Next, the cells were immobilized with 4% paraformaldehyde

for 10 min. The cell nucleus and lysosomes were stained with 4,6-diamidino-2-phenylindole and Lyso Tracker, respectively. Finally, the stained cells were imaged using ZEISS inverted fluorescence microscope.

**Determination of Cytokine Levels.** THP-1 cells were seeded at a density of  $1.0 \times 10^5$  cells per well in a 96-well culture plate and treated with 20 ng/mL PMA in order to differentiate into macrophage-like THP-1 (dTHP-1) cells. After, the medium was replaced with 100 μL of serum-free medium containing different concentrations of nanosheets or the corona complexes (0, 12.5, 25, and 50 μg/mL) for 12 h. Then, the supernatant was reserved for the levels of cytokines (IL-1β, IL-6, IFN-γ, and IL-8) assay by ELISA kits. All experiments were performed three times to ensure repeatability of the results.

**Measurement of ROS in Macrophages.** THP-1 cells were seeded at a density of  $1.0 \times 10^5$  cells per well in a 96-well culture plate and treated with 20 ng/mL PMA in order to differentiate into macrophage-like THP-1 (dTHP-1) cells. The culture medium was replaced with 100 μL of DMEM medium containing DCF-DA and incubated at 37 °C for 30 min. Next, these nanosheets and the corona complexes were added to the wells at 50 μg/mL. The fluorescence intensity of DMEM medium contained DCF-DA was measured by a Tecan InfiniteM1000 PRO enzyme marker with excitation and emission wavelengths of 488 and 525 nm, respectively, and the fluorescence intensity was used to evaluate the ROS level in dTHP-1 cells. All experiments were performed three times to ensure repeatability of the results.

## ■ ASSOCIATED CONTENT

### Supporting Information

The Supporting Information is available free of charge at <https://pubs.acs.org/doi/10.1021/acsabm.0c00306>.

Figures of TEM and SEM images, DLS analysis, stability of complexes, adsorption capacity, proteins classified by molecular weight and isoelectric point, and cytokines secretion and tables of most abundant corona proteins detectable and lists of detailed immune system processes (PDF)

## ■ AUTHOR INFORMATION

### Corresponding Authors

**Jing Zhao** – State Key Laboratory of Coordination Chemistry, Chemistry and Biomedicine Innovation Center (ChemBIC), School of Chemistry and Chemical Engineering, Nanjing University, Nanjing 210093, China; [orcid.org/0000-0001-5177-5699](https://orcid.org/0000-0001-5177-5699); Email: [jingzhao@nju.edu.cn](mailto:jingzhao@nju.edu.cn)

**Chongjiang Cao** – Department of Food Quality and Safety/National R&D Center for Chinese Herbal Medicine Processing, College of Engineering, China Pharmaceutical University, Nanjing 211198, China; [orcid.org/0000-0001-6160-1166](https://orcid.org/0000-0001-6160-1166); Email: [cj33@163.com](mailto:cj33@163.com)

### Authors

**Miaomiao Han** – Department of Food Quality and Safety/National R&D Center for Chinese Herbal Medicine Processing, College of Engineering, China Pharmaceutical University, Nanjing 211198, China; State Key Laboratory of Coordination Chemistry, Chemistry and Biomedicine Innovation Center (ChemBIC), School of Chemistry and Chemical Engineering, Nanjing University, Nanjing 210093, China

**Longqian Zhu** – State Key Laboratory of Coordination Chemistry, Chemistry and Biomedicine Innovation Center (ChemBIC), School of Chemistry and Chemical Engineering, Nanjing University, Nanjing 210093, China

**Jianbin Mo** – State Key Laboratory of Coordination Chemistry, Chemistry and Biomedicine Innovation Center (ChemBIC),

School of Chemistry and Chemical Engineering, Nanjing University, Nanjing 210093, China

**Wei Wei** – State Key Laboratory of Coordination Chemistry, Chemistry and Biomedicine Innovation Center (ChemBIC), School of Chemistry and Chemical Engineering, Nanjing University, Nanjing 210093, China

**Biao Yuan** – Department of Food Quality and Safety/National R&D Center for Chinese Herbal Medicine Processing, College of Engineering, China Pharmaceutical University, Nanjing 211198, China

Complete contact information is available at:  
<https://pubs.acs.org/10.1021/acsabm.0c00306>

### Author Contributions

M.H. and L.Z. carried out the experimental works; M.H., J.M., and W.W. wrote the manuscript; J.Z., C.C., and B.Y. guided the project.

### Notes

The authors declare no competing financial interest.

### ACKNOWLEDGMENTS

This work was financially supported by National Key Research and Development Program of China (2018YFD0901106), the National Science Foundation of China (31972118, 21622103, and 21671099), Natural Science Foundation of Jiangsu Province (BK20180008), and National Key R&D Program of China (2017YFA0208200).

### REFERENCES

- (1) Mannix, A. J.; Zhou, X. F.; Kiraly, B.; Wood, J. D.; Alducin, D.; Myers, B. D.; Liu, X.; Fisher, B. L.; Santiago, U.; Guest, J. R.; et al. Synthesis of borophenes: Anisotropic, two-dimensional boron polymorphs. *Science* **2015**, *350* (6267), 1513.
- (2) Li, H.; Jing, L.; Liu, W.; Lin, J.; Tay, R. Y.; Tsang, S. H.; Teo, E. H. T. Scalable Production of Few-Layer Boron Sheets by Liquid-Phase Exfoliation and Their Superior Supercapacitive Performance. *ACS Nano* **2018**, *12* (2), 1262–1272.
- (3) Mannix, A. J.; Zhang, Z.; Guisinger, N. P.; Yakobson, B. I.; Hersam, M. C. Borophene as a prototype for synthetic 2D materials development. *Nat. Nanotechnol.* **2018**, *13* (6), 444–450.
- (4) Molle, A.; Goldberger, J.; Houssa, M.; Xu, Y.; Zhang, S. C.; Akinwande, D. Buckled two-dimensional Xene sheets. *Nat. Mater.* **2017**, *16* (2), 163.
- (5) Ranjan, P.; Sahu, T. K.; Bhushan, R.; Yamijala, S. S.; Late, D. J.; Kumar, P.; Vinu, A. Freestanding Borophene and Its Hybrids. *Adv. Mater.* **2019**, *31* (27), No. 1900353.
- (6) Sun, X.; Liu, X.; Yin, J.; Yu, J.; Li, Y.; Hang, Y.; Zhou, X.; Yu, M.; Li, J.; Tai, G.; Guo, W. Two-Dimensional Boron Crystals: Structural Stability, Tunable Properties, Fabrications and Applications. *Adv. Funct. Mater.* **2017**, *27* (19), 1603300.
- (7) Zhang, X.; Wu, T.; Wang, H.; Zhao, R.; Chen, H.; Wang, T.; Wei, P.; Luo, Y.; Zhang, Y.; Sun, X. Boron Nanosheet: An Elemental Two-Dimensional (2D) Material for Ambient Electrocatalytic N<sub>2</sub>-to-NH<sub>3</sub> Fixation in Neutral Media. *ACS Catal.* **2019**, *9* (5), 4609–4615.
- (8) Xie, S. Y.; Wang, Y.; Li, X. B. Flat Boron: A New Cousin of Graphene. *Adv. Mater.* **2019**, *31* (36), No. 1900392.
- (9) Cheng, L.; Wang, X.; Gong, F.; Liu, T.; Liu, Z. 2D Nanomaterials for Cancer Theranostic Applications. *Adv. Mater.* **2020**, *32*, 1902333.
- (10) Luo, M.; Fan, T.; Zhou, Y.; Zhang, H.; Mei, L. 2D Black Phosphorus-Based Biomedical Applications. *Adv. Funct. Mater.* **2019**, *29* (13), No. 1808306.
- (11) Tao, W.; Kong, N.; Ji, X.; Zhang, Y.; Sharma, A.; Ouyang, J.; Qi, B.; Wang, J.; Xie, N.; Kang, C.; Zhang, H.; Farokhzad, O. C.; Kim, J. S. Emerging two-dimensional monoelemental materials (Xenes) for biomedical applications. *Chem. Soc. Rev.* **2019**, *48* (11), 2891–2912.
- (12) Chen, W.; Ouyang, J.; Liu, H.; Chen, M.; Zeng, K.; Sheng, J.; Liu, Z.; Han, Y.; Wang, L.; Li, J.; Deng, L.; Liu, Y. N.; Guo, S. Black Phosphorus Nanosheet-Based Drug Delivery System for Synergistic Photodynamic/Photothermal/Chemotherapy of Cancer. *Adv. Mater.* **2017**, *29* (5), 1603864.
- (13) Shao, J.; Xie, H.; Huang, H.; Li, Z.; Sun, Z.; Xu, Y.; Xiao, Q.; Yu, X.-F.; Zhao, Y.; Zhang, H.; Wang, H.; Chu, P. K. Biodegradable black phosphorus-based nanospheres for in vivo photothermal cancer therapy. *Nat. Commun.* **2016**, *7* (1), 12967.
- (14) Yang, B.; Yin, J.; Chen, Y.; Pan, S.; Yao, H.; Gao, Y.; Shi, J. 2D-Black-Phosphorus-Reinforced 3D-Printed Scaffolds: A Stepwise Countermeasure for Osteosarcoma. *Adv. Mater.* **2018**, *30* (10), 1705611.
- (15) Ji, X.; Kong, N.; Wang, J.; Li, W.; Xiao, Y.; Gan, S. T.; Zhang, Y.; Li, Y.; Song, X.; Xiong, Q.; Shi, S.; Li, Z.; Tao, W.; Zhang, H.; Mei, L.; Shi, J. A Novel Top-Down Synthesis of Ultrathin 2D Boron Nanosheets for Multimodal Imaging-Guided Cancer Therapy. *Adv. Mater.* **2018**, *30*, 1870268.
- (16) Monopoli, M. P.; Aberg, C.; Salvati, A.; Dawson, K. A. Biomolecular coronas provide the biological identity of nanosized materials. *Nat. Nanotechnol.* **2012**, *7* (12), 779–786.
- (17) Cedervall, T.; Lynch, I.; Lindman, S.; Berggard, T.; Thulin, E.; Nilsson, H.; Dawson, K. A.; Linse, S. Understanding the nanoparticle-protein corona using methods to quantify exchange rates and affinities of proteins for nanoparticles. *Proc. Natl. Acad. Sci. U. S. A.* **2007**, *104* (7), 2050–2055.
- (18) Cai, R.; Chen, C. The Crown and the Scepter: Roles of the Protein Corona in Nanomedicine. *Adv. Mater.* **2019**, *31*, 1805740.
- (19) Wang, L.; Li, J.; Pan, J.; Jiang, X.; Ji, Y.; Li, Y.; Qu, Y.; Zhao, Y.; Wu, X.; Chen, C. Revealing the Binding Structure of the Protein Corona on Gold Nanorods Using Synchrotron Radiation-Based Techniques: Understanding the Reduced Damage in Cell Membranes. *J. Am. Chem. Soc.* **2013**, *135* (46), 17359–17368.
- (20) Wang, X.; Wang, X.; Wang, M.; Zhang, D.; Chen, C.; et al. Probing Adsorption Behaviors of BSA onto Chiral Surfaces of Nanoparticles. *Small* **2018**, *14* (16), 1703982.
- (21) Ren, J.; Cai, R.; Wang, J.; Daniyal, M.; Chen, C.; et al. Precision Nanomedicine Development Based on Specific Opsonization of Human Cancer Patient-Personalized Protein Coronas. *Nano Lett.* **2019**, *19* (7), 4692–4701.
- (22) Monopoli, M. P.; Walczyk, D.; Campbell, A.; Elia, G.; Lynch, I.; Baldelli Bombelli, F.; Dawson, K. A. Physical-Chemical Aspects of Protein Corona: Relevance to in Vivo Biological Impacts of Nanoparticles. *J. Am. Chem. Soc.* **2011**, *133* (8), 2525–2534.
- (23) Tenzer, S.; Docter, D.; Kuharev, J.; Musyanovych, A.; Fetz, V.; Hecht, R.; Schlenk, F.; Fischer, D.; Kiouptsi, K.; Reinhardt, C.; Landfester, K.; Schild, H.; Maskos, M.; Knauer, S. K.; Stauber, R. H. Rapid formation of plasma protein corona critically affects nanoparticle pathophysiology. *Nat. Nanotechnol.* **2013**, *8* (10), 772–81.
- (24) Walkey, C. D.; Olsen, J. B.; Guo, H.; Emili, A.; Chan, W. C. Nanoparticle size and surface chemistry determine serum protein adsorption and macrophage uptake. *J. Am. Chem. Soc.* **2012**, *134* (4), 2139–47.
- (25) Lee, C.; Wei, X.; Kysar, J. W.; Hone, J. Measurement of the elastic properties and intrinsic strength of monolayer graphene. *Science* **2008**, *321* (5887), 385–8.
- (26) Loh, K. P.; Bao, Q.; Ang, P. K.; Yang, J. The chemistry of graphene. *J. Mater. Chem.* **2010**, *20* (12), 2277–2289.
- (27) Ye, X.; Liang, X.; Chen, Q.; Miao, Q.; Chen, X.; Zhang, X.; Mei, L. Surgical tumor-derived personalized photothermal vaccine formulation for cancer immunotherapy. *ACS Nano* **2019**, *13*, 2956–2968.
- (28) Liang, X.; Ye, X.; Wang, C.; Xing, C.; Miao, Q.; Xie, Z.; Chen, X.; Zhang, X.; Zhang, H.; Mei, L. Photothermal cancer immunotherapy by erythrocyte membrane-coated black phosphorus formulation. *J. Controlled Release* **2019**, *296*, 150–161.
- (29) Liu, G.; Tsai, H.-I.; Zeng, X.; Qi, J.; Luo, M.; Wang, X.; Mei, L.; Deng, W. Black phosphorus nanosheets-based stable drug delivery system via drugself-stabilization for combined photothermal and chemo cancer therapy. *Chem. Eng. J.* **2019**, *375*, 121917.

- (30) Zeng, X.; Luo, M.; Liu, G.; Wang, X.; Tao, W.; Lin, Y.; Ji, X.; Nie, L.; Mei, L. Polydopamine-Modified Black Phosphorous Nanocapsule with Enhanced Stability and Photothermal Performance for Tumor Multimodal Treatments. *Adv. Sci. (Weinh)* **2018**, *5* (10), 1800510.
- (31) Castagnola, V.; Zhao, W.; Boselli, L.; Lo Giudice, M. C.; Meder, F.; Polo, E.; Paton, K. R.; Backes, C.; Coleman, J. N.; Dawson, K. A. Biological recognition of graphene nanoflakes. *Nat. Commun.* **2018**, *9* (1), 1577.
- (32) Mo, J.; Xie, Q.; Wei, W.; Zhao, J. Revealing the immune perturbation of black phosphorus nanomaterials to macrophages by understanding the protein corona. *Nat. Commun.* **2018**, *9* (1), 2480.
- (33) Zhang, H.; Burnum, K. E.; Luna, M. L.; Petritis, B. O.; Jong-Seo, K.; Wei-Jun, Q.; Moore, R. J.; Alejandro, H. L.; Webb-Robertson, B. J. M.; Thrall, B. D.; et al. Quantitative proteomics analysis of adsorbed plasma proteins classifies nanoparticles with different surface properties and size. *Proteomics* **2011**, *11* (23), 4569–4577.
- (34) Monopoli, M. P.; Åberg, C.; Salvati, A.; Dawson, K. A. Biomolecular coronas provide the biological identity of nanosized materials. *Nat. Nanotechnol.* **2012**, *7* (12), 779–786.
- (35) Casals, E.; Pfaller, T.; Duschl, A.; Oostingh, G. J.; Puntès, V. Time Evolution of the Nanoparticle Protein Corona. *ACS Nano* **2010**, *4* (7), 3623–32.
- (36) Monopoli, M. P.; Åberg, C.; Salvati, A.; Dawson, K. A. Biomolecular coronas provide the biological identity of nanosized materials. *Nat. Nanotechnol.* **2012**, *7* (12), 779–86.
- (37) Pondman, K. M.; Pednekar, L.; Paudyal, B.; Tsolaki, A. G.; Kouser, L.; Khan, H. A.; Shamji, M. H.; Haken, B. T.; Stenbeck, G.; Sim, R. B.; et al. Innate immune humoral factors, C1q and factor H, with differential pattern recognition properties, alter macrophage response to carbon nanotubes. *Nanomedicine* **2015**, *11* (8), 2109–2118.
- (38) Zhao, F.; Zhao, Y.; Liu, Y.; Chang, X.; Chen, C.; Zhao, Y. Cellular Uptake, Intracellular Trafficking, and Cytotoxicity of Nanomaterials. *Small* **2011**, *7* (10), 1322–1337.
- (39) Guiney, L. M.; Wang, X.; Xia, T.; Nel, A. E.; Hersam, M. C. Assessing and Mitigating the Hazard Potential of Two-Dimensional Materials. *ACS Nano* **2018**, *12* (7), 6360–6377.
- (40) Seabra, A. B.; Paula, A. J.; de Lima, R.; Alves, O. L.; Duran, N. Nanotoxicity of graphene and graphene oxide. *Chem. Res. Toxicol.* **2014**, *27* (2), 159–68.
- (41) Neagu, M.; Piperigkou, Z.; Karamanou, K.; Engin, A. B.; Docea, A. O.; Constantin, C.; Negrei, C.; Nikitovic, D.; Tsatsakis, A. Protein bio-corona: critical issue in immune nanotoxicology. *Arch. Toxicol.* **2017**, *91* (3), 1031–1048.
- (42) Guan, G.; Zhang, S.; Liu, S.; Cai, Y.; Low, M.; Teng, C. P.; Phang, I. Y.; Cheng, Y.; Duei, K. L.; Srinivasan, B. M.; et al. Protein Induces Layer-by-Layer Exfoliation of Transition Metal Dichalcogenides. *J. Am. Chem. Soc.* **2015**, *137* (19), 6152–6155.
- (43) Wang, L.; Quan, P.; Chen, S. H.; Bu, W.; Chen, C.; et al. Stability of Ligands on Nanoparticles Regulating the Integrity of Biological Membranes at Nano-Lipid Interface. *ACS Nano* **2019**, *13* (8), 8680–8693.
- (44) Chinen, A. B.; Guan, C. M.; Ko, C. H.; Mirkin, C. A. The Impact of Protein Corona Formation on the Macrophage Cellular Uptake and Biodistribution of Spherical Nucleic Acids. *Small* **2017**, *13* (16), 1603847.
- (45) Lesniak, A.; Fenaroli, F.; Monopoli, M. P.; Åberg, C.; Dawson, K. A.; Salvati, A. Effects of the Presence or Absence of a Protein Corona on Silica Nanoparticle Uptake and Impact on Cells. *ACS Nano* **2012**, *6* (7), 5845–5857.
- (46) Elsabahy, M.; Wooley, K. L. Cytokines as biomarkers of nanoparticle immunotoxicity. *Chem. Soc. Rev.* **2013**, *42* (12), 5552.
- (47) Dobrovolskaia, M. A.; Germolec, D. R.; Weaver, J. L. Evaluation of nanoparticle immunotoxicity. *Nat. Nanotechnol.* **2009**, *4* (7), 411–414.
- (48) Corbo, C.; Molinaro, R.; Parodi, A.; Furman, N. E. T.; Salvatore, F.; Tasciotti, E. The impact of nanoparticle protein corona on cytotoxicity, immunotoxicity and target drug delivery. *Nanomedicine* **2016**, *11* (1), 81–100.
- (49) Zhou, H.; Zhao, K.; Li, W.; Yang, N.; Liu, Y.; Chen, C.; Wei, T. The interactions between pristine graphene and macrophages and the production of cytokines/chemokines via TLR- and NF- $\kappa$ B-related signaling pathways. *Biomaterials* **2012**, *33* (29), 6933–6942.
- (50) Moyano, D. F.; Goldsmith, M.; Solfiell, D. J.; Landesman-Milo, D.; Miranda, O. R.; Peer, D.; Rotello, V. M. Nanoparticle hydrophobicity dictates immune response. *J. Am. Chem. Soc.* **2012**, *134* (9), 3965–3967.
- (51) Gao, N.; Zhang, Q.; Mu, Q.; Bai, Y.; Li, L.; Zhou, H.; Butch, E. R.; Powell, T. B.; Snyder, S. E.; Jiang, G.; Yan, B. Steering Carbon Nanotubes to Scavenger Receptor Recognition by Nanotube Surface Chemistry Modification Partially Alleviates NF $\kappa$ B Activation and Reduces Its Immunotoxicity. *ACS Nano* **2011**, *5* (6), 4581–4591.
- (52) Old, L. Tumor necrosis factor (TNF). *Science* **1985**, *230* (4726), 630–632.
- (53) Nel, A.; Xia, T.; Mdlar, L.; Li, N. Toxic Potential of Materials at the Nanolevel. *Science* **2006**, *311* (5761), 622–627.